High pressure effects on isotropic Nd2Fe14B magnet accompanying change in coercive field

High pressure effects on isotropic $Nd_2Fe_{14}B$ magnet accompanying change in coercive field

Cite as: J. Appl. Phys. **118**, 145901 (2015); https://doi.org/10.1063/1.4932599
Submitted: 11 July 2015 . Accepted: 25 September 2015 . Published Online: 09 October 2015

M. Mito, H. Goto, K. Nagai, K. Tsuruta, H. Deguchi, T. Tajiri, and K. Konishi

High pressure effects on isotropic $Nd_2Fe_{14}B$ magnet accompanying change in coercive field

M. Mito,[1,a)] H. Goto,[1] K. Nagai,[1] K. Tsuruta,[1] H. Deguchi,[1] T. Tajiri,[2] and K. Konishi[3]
[1]*Graduate School of Engineering, Kyushu Institute of Technology, Kitakyushu 804-8550, Japan*
[2]*Faculty of Science, Fukuoka University, Fukuoka 814-0180, Japan*
[3]*Graduate School of Science and Engineering, Ehime University, Matsuyama 790-8577, Japan*

(Received 11 July 2015; accepted 25 September 2015; published online 9 October 2015)

We investigated the effects of hydrostatic pressure on an isotropic $Nd_2Fe_{14}B$ magnet (the exact chemical formula is $Nd_{2.0}Fe_{14.1}B$) consisting of nanocrystals, with the size of approximately 30 nm, by magnetization measurements at pressures (P's) up to 9.3 GPa and structural analyses up to 4.3 GPa. Magnetization curves were measured by using a miniature diamond anvil cell made of Ti alloy with spatially uniform magnetization. The initial value of coercive field H_c at 300 K is 840 kA/m (=10.6 kOe), and H_c initially increases to approximately 1180 kA/m (=15.0 kOe) almost linearly against the pressure. The increase in H_c, however, saturates at around $P = 3$ GPa. The change in H_c is understood by the decrease in the saturation magnetization M_s within the framework of the constant anisotropy of the single domain phase. The crystalline strain increases for $P < 1$ GPa. Afterward, the crystalline size (D) starts to decrease with increasing pressure, and the reduction tends to saturate at above approximately 3 GPa. Furthermore, the change in M_s is actually related with both the change in strain and that in D. The data on the temperature dependence of H_c at $P = 0$, 6.6, and 9.3 GPa exhibit pressure-induced suppression of the Curie temperature. The maximum energy product decreases with increasing pressure over the whole temperature range. © *2015 AIP Publishing LLC*. [http://dx.doi.org/10.1063/1.4932599]

I. INTRODUCTION

The creation of powerful permanent magnets is an industrially important theme for achieving a low-energy society. The $Nd_2Fe_{14}B$ magnet is currently one of the most attractive permanent magnets with high coercive field (H_c), as it has the largest magnetic moment among $R_2Fe_{14}B$ compounds (where R is a rare earth element).[1–3] The ferromagnetic transition temperature (T_C) of $Nd_2Fe_{14}B$ is generally recognized as 586 K.[1,3] The main phase has the space group $P4_2/mnm$, with $a = 8.80$ Å and $c = 12.19$ Å, and there are four $Nd_2Fe_{14}B$ units per unit cell.[3,4] To utilize a $Nd_2Fe_{14}B$ magnet at high temperatures (e.g., for a car engine), it is necessary to disrupt the decrease in H_c at around 500 K.

Real $Nd_2Fe_{14}B$ magnets are divided into two types: sintered magnets and isotropic magnets. In sintered magnets, the insertion of Dy at the Fe site is an effective method of enhancing H_c at around 500 K, and the Nd-rich amorphous nonmagnetic phase appearing at the grain boundaries disturbs the nucleation for domain reversal. However, the route for obtaining Dy has been restricted, and the high-H_c $Nd_2Fe_{14}B$ magnets without including Dy are desirable. However, rapid solidification by a melt-spinning process produces "an isotropic bond magnet" with a grain size of less than 1 μm. As the grain size decreases, the coercive field generally increases. For the grain size of less than 0.3 μm, it has been experimentally known that the single magnetic domain structure is stabilized.[5] According to an electron microscopy characterization, the $Nd_2Fe_{14}B$ grains (termed *the main phase* above) are surrounded by thin amorphous films of Nd rich and B deficient phase.[6] This phase can act as a pinning site for the magnetic domain walls. Indeed, the H_c value of isotropic magnets is generally lower than that of sintered magnets. In order to increase the H_c value of isotropic magnets, there are considered four types of improvements, applied to the crystal, grain, grain boundary, and piece.

In bulky materials, H_c is generally expressed by the Kronmüller equation

$$H_c = \alpha H_a - N_{eff} M_s, \tag{1}$$

where α and N_{eff} are microstructural parameters due to defects and grain boundaries, N_{eff} denotes the effective demagnetization coefficient of the crystal particles, and M_s is the saturated magnetization.[7,8] An anisotropic field H_a is theoretically related to both an anisotropic constant K_u and M_s as

$$H_a = 2K_u/M_s. \tag{2}$$

In a sintered $Nd_2Fe_{14}B$ magnet, $\alpha = 0.37$ and $N_{eff} = 1$.[8] The magnetic curve for a single-domain particle is understood via the Stoner-Wohlfarth (SW) model.[9] For a nanocrystalline sample, the demagnetization contribution can be neglected, so that H_c can be considered to be governed by K_u and M_s.

The effect of shock wave compression on the strain in the $Nd_2Fe_{14}B$ magnet was investigated recently,[10] and the effect of loading at low temperature for rapidly quenched $Nd_2Fe_{14}B$ nanocrystalline magnets has also been studied.[11] Thus, from the viewpoint of basic physics, the effect of strain on $Nd_2Fe_{14}B$ magnets has been attractive. In 1987, the change in T_C against the pressure (P) for a polycrystalline sample,

a)Electronic address: mitoh@mns.kyutech.ac.jp

$dT_C/dP = -26.5$ K/GPa, was investigated by Kamarad *et al.*[12] In amorphous $Nd_2Fe_{14}B$ [T_C $(P=0) = 422$ K], $dT_C/dP = -48$ K/GPa.[13] However, there has never been the study for the pressure effect on H_c. Indeed, magnetization measurements at high pressure of gigapascal level and high magnetic field have been technically difficult.[14] Thus, we have developed a special diamond anvil cell for the present magnetic measurements. Now, isotropic bond magnets are suitable for attempting to change H_c by manipulating the structure of the main phase. Given these background, we investigate the change in H_c under hydrostatic pressure for an isotropic $Nd_2Fe_{14}B$ magnet and examine the magneto-structural correlation as a function of pressure.

II. EXPERIMENTAL PROCEDURES

A target $Nd_2Fe_{14}B$ bond magnet is called MQP-B 20052-070 ($Nd_{2.0}Fe_{14.1}B$; MQP, Magnequench, A Division of Neo Material Technologies Inc.); this magnet is used as the spindle motor in hard disks, power tools, and so on. The density is 7.61 ± 0.20 g/cm^3. A scanning electron microscopy (SEM) image is shown in the inset of Fig. 1. The median size of the nanoparticles aggregated at the sample surface, observed from the SEM image, is approximately 60 nm. The crystalline size D in the whole sample is evaluated to be approximately 30 nm in later structural experiment.

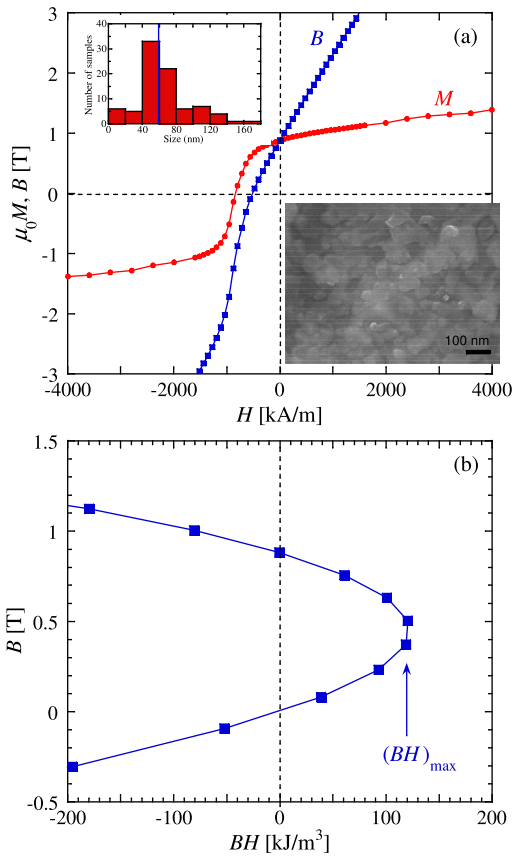

FIG. 1. (a) Magnetization curve of $Nd_{2.0}Fe_{14.1}B$ at 300 K. Inset of (a) shows SEM image of $Nd_{2.0}Fe_{14.1}B$, along with the histogram of the crystal size: In the histogram, the blue line presents the median size. The nanocrystals of about 60 nm diameter are aggregated at the surface. (b) Magnetic flux density (B) as a function of the energy product, BH. The horizontal coordinate of the extreme position of the parabolic curve yields the maximum energy product $(BH)_{max}$.

We measured the magnetization M versus the magnetic field H as a function of temperature T using a superconducting quantum interference device (SQUID) magnetometer (Quantum Design Inc.). In this paper, H is evaluated by using the MKSA unit, A/m. By multiplying the vacuum permeability μ_0 into the magnetization M, both $\mu_0 M$ and the magnetic flux density B defined as $B = \mu_0 (M + H)$ are evaluated by the MKSA unit, T. The initial H_c value at 300 K is 840 kA/m (=10.6 kOe), as seen in the magnetization curve of $Nd_{2.0}Fe_{14.1}B$ (see Fig. 1(a)). The maximum energy product $(BH)_{max}$ is 120 kJ/m^3 that is consistent with the value in opened reference data (see Fig. 1(b)).

A decade ago, we developed a miniature diamond anvil cell (mDAC) made of CuBe for a commercial SQUID magnetometer.[14] However, the magnetic inhomogeneity of commercial CuBe is inconvenient for magnetic measurement accompanied by the sample movement in the detection coil. Indeed, by locating a ferromagnetic dummy such as Co on a gasket to obtain the symmetric SQUID response,[15] we conducted the M-T measurements[16–19] and M-H measurements.[15,16] However, the drastic change in the SQUID response as a function of H, especially below a few kilooersteds, and furthermore the existence of a ferromagnetic dummy make it difficult to measure the hysteresis curve. For the present $Nd_2Fe_{14}B$ magnets, the data on the M-H hysteresis curve are quite important. Therefore, we developed an mDAC made of a Ti alloy (NSK Ltd.) with a uniform spatial distribution of the magnetic moment (see supplementary figure S1[20]), which was developed for bearings by NSK Ltd., and has better thermal conductivity than CuBe. The hardness of this Ti alloy is 450–500 Hv, which is higher than that of CuBe, 420–450 Hv. The magnetic moment of the Ti alloy depends very little on the temperature, whereas that of CuBe exhibits paramagnetism at low temperatures. At $T = 5$ K and $H = 0.1$ T, the magnetic moment per volume of the Ti alloy is approximately six times that of CuBe and two-fifths that of pure Ti. The design of the Ti alloy mDAC is the same as that of the CuBe mDAC.[14] The pressure value was estimated by measuring the fluorescence of ruby,[21] located at the sample cavity along with the nanocrystals of $Nd_{2.0}Fe_{14.1}B$ and Apiezon-J oil as the pressure-transmitting medium.

Powder X-ray diffraction (XRD) analysis under pressures was conducted at room temperature using a synchrotron radiation XRD system with a cylindrical imaging plate at the Photon Factory (PF) at the Institute of Materials Structure Science, High Energy Accelerator Research Organization (KEK).[22] The wavelength of the incident X-ray was 0.88571 Å. Pressure was applied using a CuBe diamond anvil cell, containing the $Nd_{2.0}Fe_{14.1}B$ nanocrystals along with a ruby as a manometer and fluorinated oil (FC77, Sumitomo 3M) as the pressure-transmitting medium.

III. EXPERIMENTAL RESULTS

Figure 2(a) shows the $\mu_0 M$–H curve of the $Nd_{2.0}Fe_{14.1}B$ bond magnet at 300 K under the following pressure changes:

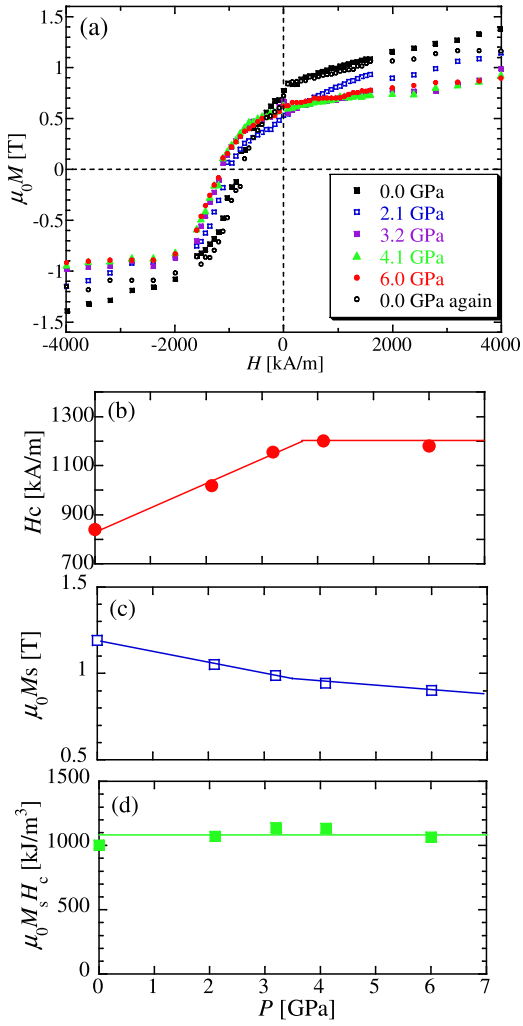

FIG. 2. (a) $\mu_0 M$-H curve of $Nd_{2.0}Fe_{14.1}B$ for 4 MA/m (= 5 kOe) → −4 MA/m at 300 K under the following pressure changes: 0 → 2.1 → 3.2 → 4.1 → 6.0 → 0 GPa. (b) H_c, (c) $\mu_0 M_s$, and (d) $\mu_0 M_s H_c$ as a function of P. The solid lines are guides for the eyes.

0 → 2.1 → 3.2 → 4.1 → 6.0 → 0 GPa. Then, the magnetic field was reduced from +4 MA/m (=5 kOe) to −4 MA/m, and the background contribution due to the mDAC was subtracted. As the pressure increased, the overall H dependence shifted toward the negative field side, suggesting an increase in H_c. The pressure dependence of three physical quantities, H_c, $\mu_0 M_s$, and their product $\mu_0 M_s H_c$, is shown in Figs. 2(b)–2(d), respectively. As for $\mu_0 M_s$, the value was estimated after subtracting the linear contribution against H. H_c increased linearly against the pressure up to 3.2 GPa, above which H_c tended to have a constant value. The H_c value after the pressure of 6.0 GPa was removed is almost the same as the initial one. However, $\mu_0 M_s$ exhibits the opposite pressure response to that of H_c and, for $P > 3.5$ GPa, $\mu_0 M_s$ also seems to approach a constant value. Their product, $\mu_0 M_s H_c$, maintains almost the same magnitude over the pressure range considered here. Theoretically, $\mu_0 M_s H_c$ represents the magnitude of the effective magnetic anisotropy K_u at the low-temperature limit. The quantitative evaluation of maximum energy product $(BH)_{max}$ is not confident at this measurement because of poor accuracy at around zero field, whereas it has been confirmed that $(BH)_{max}$ tends to decrease with increasing pressure. The behavior described above suggests that the effective anisotropy within the nanocrystalline system changes very little in the considered pressure region. Thus, the increase in H_c is triggered by the reduction of M_s with a stable K_u within the framework of the SW model. These changes in M_s and $M_s H_c$ as well as H_c have been observed in another isotropic magnet MQP-B 10184-070 ($Nd_{2.3}CoFe_{14.7}B$) (see supplementary figures S2 and S3[20]). Furthermore, the abovementioned behavior has also been seen in Nd-Fe-B sintered magnets with addition of Dy.[23,24]

Figures 3(a)–3(c) show the $\mu_0 M$–H curves of $Nd_{2.0}Fe_{14.1}B$ as a function of T for $P = 0$, 6.6, and 9.3 GPa. Figure 4 shows the temperature dependence of H_c and $(BH)_{max}$ for $P = 0$, 6.6, and 9.3 GPa, suggesting that T_C is reduced by pressure. Here, we define the critical temperature at $H_c \neq 0$ that should be less than T_C, and the value at $P = 0$ GPa is consistent with the literature value of T_C. Hereafter, the above critical temperature is defined as T_C. T_C at $P = 0$, 6.6, and 9.3 GPa, obtained by extrapolating H_c (T), is 586 ± 10 K, 480 ± 20 K, and 420 ± 10 K, respectively. Consequently, $dT_C/dP = -17.8$ K/GPa.

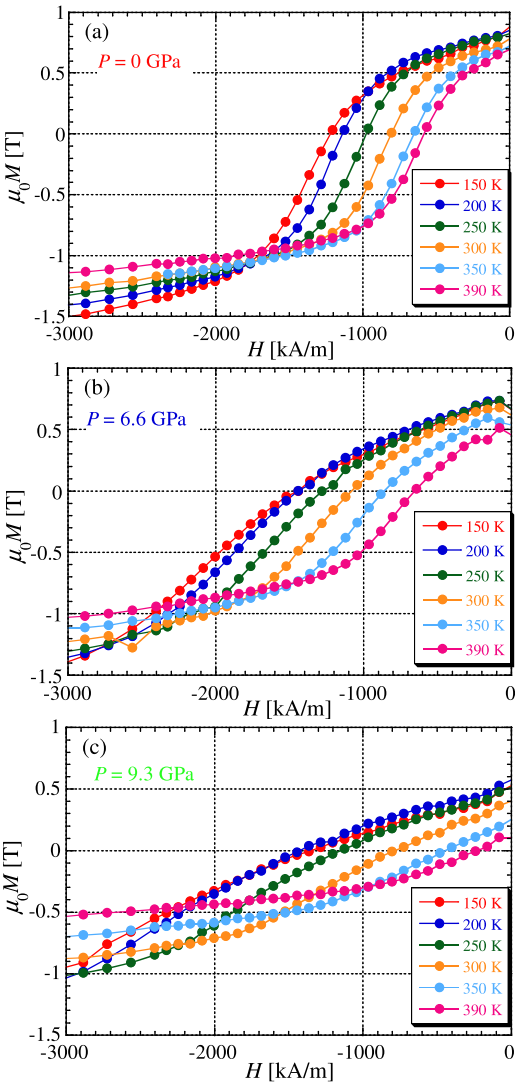

FIG. 3. (a)–(c) $\mu_0 M$-H curve of $Nd_{2.0}Fe_{14.1}B$ for 0 → −3 MA/m in the process of 4 MA/m (= 5 kOe) → −4 MA/m at various temperatures for $P = 0$ (a), 6.6 GPa (b), and 9.3 GPa (c). The solid curves are guides for the eyes.

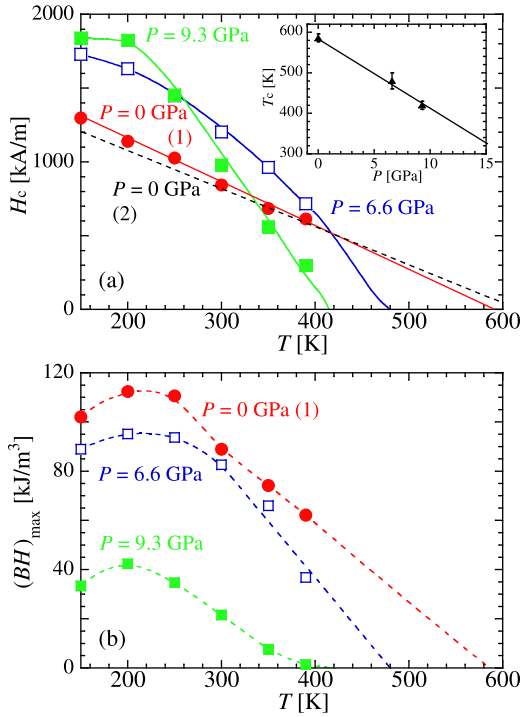

FIG. 4. (a) Temperature dependence of H_c for $P = 0$, 6.6, and 9.3 GPa along with the pressure dependence of the Curie temperature T_C. (b) Temperature dependence of $(BH)_{max}$ for $P = 0$, 6.6, and 9.3 GPa.

It is convincing that the magnitude of the decrease in T_C is smaller than a previously reported value for T_C of a polycrystalline sample ($dT_C/dP = -26.5$ K/GPa).[12] $(BH)_{max}$ systematically decreases as increasing pressure over the whole temperature. The industrial performance is reduced by applying pressure.

Figure 5 shows the XRD pattern at room temperature for $Nd_{2.0}Fe_{14.1}B$. We also estimated the crystallite size D and strain according to the Williamson-Hall plot, and their results are shown in Fig. 6. At $P = 0$ GPa, the crystallite size D was estimated to be 27.5 ± 2.8 nm. For $P < 1$ GPa, the strain is enhanced, whereas for $P > 1$ GPa, the magnitude tends to be saturated. After the saturation of the strain magnitude, D begins to decrease and, for $P > 3$ GPa, its reduction also tends to be saturated. Indeed, both the saturation of the increase in H_c and the saturation in the change in D occur at the same pressure of approximately 3 GPa. Thus, the series of increases in H_c in Fig. 2(b) should be characterized as the effects of both the increase in strain and the decrease in D. We consider that by applying pressure, some atomic sites deviate from the positions with translation symmetry, resulting in the reduction in crystallinity. This influence appears in the lattice parameters and in D. Figure 7 also shows the pressure dependence of the lattice parameters obtained via the peak angles of the distinguishable diffraction peaks. For $P \leq 1.7$ GPa, contraction within the *ab* plane is dominant, whereas for $P > 1.7$ GPa, the volume contraction originates in contraction along the *c*-axis rather than that within the *ab* plane (see Fig. 8).

IV. DISCUSSION

As shown in Fig. 2, the increase in H_c for $Nd_{2.0}Fe_{14.1}B$ at room temperature appears for $P \leq 6$ GPa, with a constant

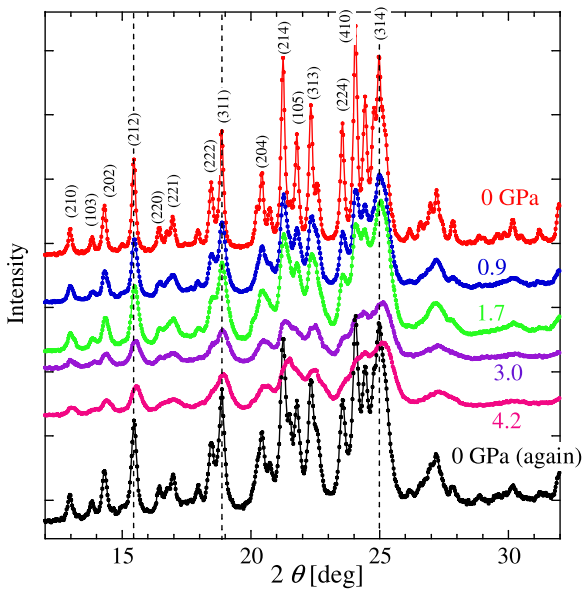

FIG. 5. Diffraction pattern of $Nd_{2.0}Fe_{14.1}B$ bond magnet for $P \leq 4.2$ GPa. The pattern at $P = 0$ GPa is explained by a crystal structure of $P4_2/mnm$ with $a = 8.795$ Å, $c = 12.188$ Å. The plane indices are presented for the diffraction peaks below $2\theta = 25°$. Three broken lines are guides to the eye to confirm the pattern shift.

value of $\mu_0 M_s H_c$. H_c is enhanced within the framework of the SW model with a constant K_u. As mentioned above, a similar phenomenon has been observed in $Nd_{2.3}CoFe_{14.7}B$ (see supplementary figure S3[20]). The addition of Co improves the Curie temperature, consequently reforming the grain

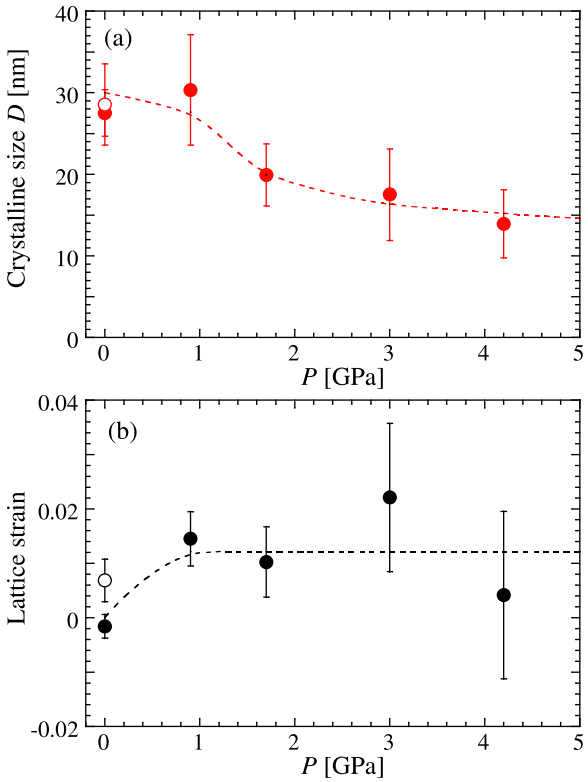

FIG. 6. Pressure dependence of crystalline size D (a) and strain (b) of $Nd_{2.0}Fe_{14.1}B$ bond magnet for $P \leq 4.2$ GPa. The broken curves are guides for the eyes. In both (a) and (b), open symbols stand for the data after releasing 4.2 GPa.

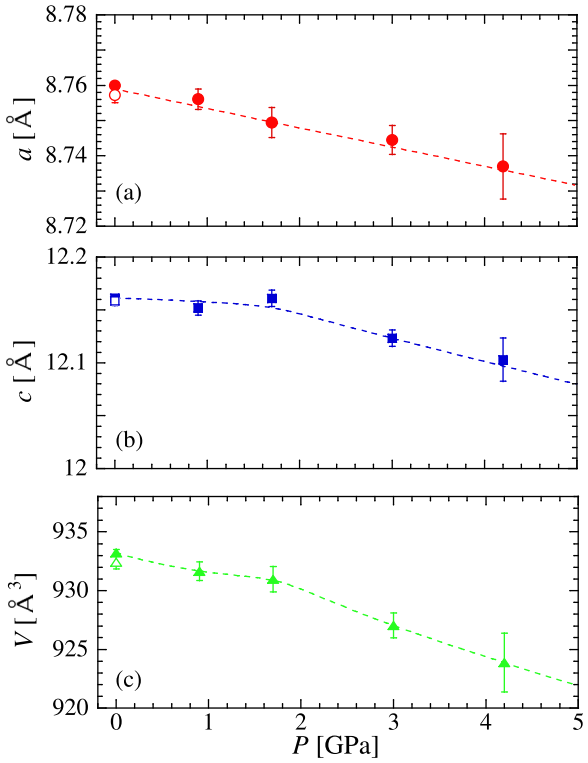

FIG. 7. Pressure dependence of the lattice parameters (a, c, V) of $Nd_{2.0}Fe_{14.1}B$ bond magnet for $P \leq 4.2$ GPa. In (a)-(c), open symbols stand for the data after releasing 4.2 GPa. The broken lines are guides for the eyes.

boundary, and improves the corrosion resistance. The grain boundary conditions differ between two materials, whereas similar phenomena have been observed. Furthermore, we recall that in $Nd_{2.0}Fe_{14.1}B$, H_c tends to saturate at a characteristic pressure, below which the crystal structure exhibits the reduction in crystallinity (i.e., the decrease in D and the increase in strain). As seen in Fig. 8, the unit cell of a $Nd_2Fe_{14}B$ magnet has many atoms, which are condensed in a narrow space (i.e., they have high density).[25] The room for structural manipulation using pressure would be small, and we can suppose that even the slight pressure brings about the

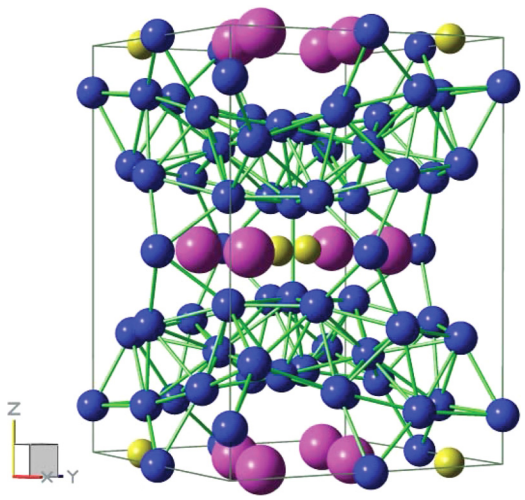

FIG. 8. Crystal structure displayed referring to the literature.[25] Purple, blue, and yellow spheres represent Nd, Fe, and B atoms, respectively.

increase in strain and the decrease in D. In particular, the latter is related with the contraction along the c-axis.

The change in H_c at 300 K occurs in the pressure region, where anisotropic shrinkage occurs, and it cannot be scaled with one lattice parameter among a, c, and V. After the change in lattice strain disappears, D starts to decrease largely. We stress that the change in H_c is the most similar to that in D among a series of structural parameters. As mentioned above, the change in D is surely related with the change in c. In order to elucidate the magneto-structural correlation, we have to pursue each atomic position at pressures. We are planning the structural analysis at pressure of below 1 GPa, where the lattice strain exhibits a prominent change. According to the literature, amorphization results in reduction of both H_c and T_C.[26] We remark that the reduction in crystallinity mainly brings about reduction of both H_c and T_C in the present study.

Indeed, the structural change accompanying the reduction in crystallinity under hydrostatic pressure reduces T_C, which degrades the performance at around 500 K. However, if we consider the magnetic properties below 400 K, the increase in H_c is realized.

V. SUMMARY

The effect of pressure on the isotropic bond magnet $Nd_{2.0}Fe_{14.1}B$ was investigated to study the potential features of the main phase for higher H_c. We observed an increase in H_c at $T = 300$ K, the magnitude of which corresponds to 40% of the initial value. The above behavior at $T = 300$ K is understood within the SW model, accompanying the decrease in M_s and the constant K_u. The temperature dependence of H_c at $P = 6.6$ and 9.3 GPa indicates that T_C decreases with the reduction in crystallinity. The increase in H_c at room temperature stops at around $P = 3.0$ GPa, where contraction along the c-axis rather than that within the ab-plane is dominant. A series of results suggests that the magnetic network survives even after the reduction in crystallinity, whereas under hydrostatic pressure, the magnetic ordering becomes unstable, finally accompanying the decrease in both H_c and M_s. Thus, there is a limit on how much H_c can be achieved by manipulating the crystal structure of the main phase under hydrostatic pressure.

ACKNOWLEDGMENTS

This work was supported by MEXT KAKENHI [Grant-in-Aid for Scientific Research (B) (No. 26289091) and Grant-in-Aid for Scientific Research on Innovative Areas "Bulk Nanostructured Metals" (No. 25102709)]. M.M. acknowledges NSK Ltd. for supplying the Ti alloy and Magnequench International for supplying the $Nd_{2.0}Fe_{14.1}B$ bond magnets and Professor M. Takezawa (Kyushu Institute of Technology) for presenting the related material.

[1]M. Sagawa, S. Fujimura, N. Togawa, H. Yamamoto, and Y. Matsuura, J. Appl. Phys. **55**, 2083 (1984).
[2]J. J. Croat, J. F. Herbst, R. W. Lee, and F. E. Pinkerton, J. Appl. Phys. **55**, 2078 (1984).
[3]J. F. Herbst, Rev. Mod. Phys. **63**, 819 (1991).

[4]J. F. Herbst, J. J. Croat, F. E. Pinkerton, and W. B. Yelon, Phys. Rev. **29**, 4176 (1984).
[5]M. Sagawa, S. Fujimura, H. Yamamoto, Y. Matsuura, S. Hirosawa, and K. Hiraga, in *Proceedings of the 8th International Workshop on Rare-Earth Magnets* (1985), p. 587.
[6]R. K. Mishra, J. Magn. Magn. Mater. **54–57**, 450–456 (1986).
[7]H. Kronmüller, Phys. Status Solidi B **144**, 385 (1987).
[8]S. Hirosawa, K. Tokuhara, Y. Matsuura, H. Yamamoto, S. Fujimura, and M. Sagawa, J. Magn. Magn. Mater. **61**, 363 (1986).
[9]E. Stoner and E. Wohlfarth, Philos. Trans. R. Soc. London, Ser. A **240**, 599 (1948).
[10]L. Yan-Feng, Z. Ming-Gang, L. Wei, Z. Dong, L. Feng, C. Lang, W. Jun-Ying, Q. Yan, and D. An, Chin. Phys. Lett. **30**, 097501 (2013).
[11]C. bing Rong, Y. Q. Wu, D. Wang, Y. Zhang, N. Poudyal, M. J. Kramer, and J. P. Liu, J. Appl. Phys. **111**, 07A717 (2012).
[12]J. Kamarad, Z. Arnold, and J. Schneider, J. Magn. Magn. Mater. **67**, 29 (1987).
[13]K. Fukamachi, K. Shirakawa, Y. Satoh, T. Masumoto, and T. Kaneko, J. Magn. Magn. Mater. **54–57**, 231–232 (1986).
[14]M. Mito, M. Hitaka, T. Kawae, K. Takeda, T. Kitai, and N. Toyoshima, Jpn. J. Appl. Phys., Part 1 **40**, 6641 (2001).
[15]G. Subias, V. Cuartero, J. Garcia, J. Blasco, S. Lafuerza, S. Pascarelli, O. Mathon, C. Strohm, K. Nagai, M. Mito *et al.*, Phys. Rev. B **87**, 094408 (2013).
[16]K. Takeda and M. Mito, J. Phys. Soc. Jpn. **71**, 729 (2002).
[17]M. Ohba, W. Kaneko, S. Kitagawa, T. Maeda, and M. Mito, J. Am. Chem. Soc. **130**, 4475 (2008).
[18]M. Mito, K. Matsumoto, Y. Komorida, H. Deguchi, S. Takagi, T. Tajiri, T. Iwamoto, T. Kawae, M. Tokita, and K. Takeda, J. Phys. Chem. Solids **70**, 1290 (2009).
[19]M. Mito, S. Yamaguchi, H. Tsuruda, H. Deguchi, and M. Ishizuka, J. Appl. Phys. **115**, 13903 (2014).
[20]See supplementary material at http://dx.doi.org/10.1063/1.4932599 for Ti alloy mDAC and MQP-B 10184-070 ($Nd_{2.3}CoFe_{14.7}B$).
[21]G. J. Piermarini, S. Block, J. D. Barnett, and R. A. Forman, J. Appl. Phys. **46**, 2774 (1975).
[22]A. Fujiwara, K. Ishii, T. Watanuki, H. Suematsu, H. Nakao, K. Ohwada, Y. Fujii, Y. Murakami, T. Mori, H. Kawada *et al.*, J. Appl. Crystallogr. **33**, 1241 (2000).
[23]D. W. Lim, H. Kato, M. Yamada, G. Kido, and Y. Nakagawa, Phys. Rev. B **44**, 10014 (1991).
[24]K. Kobayashi and K. Koyama, in *2009 Annual Report* (HFLSM, Institute of Material Research, Tohoku University, 2010), pp. 98–101.
[25]H. S. Li, R. C. Mohanty, A. Raman, and C. G. Grenier, J. Magn. Magn. Mater. **162**, 301 (1996).
[26]A. Teplykh, Y. Chukalkin, S. Lee, S. Bogdanov, N. Kudrevatykh, E. Rosenfeld, Y. Skryabin, Y. Choi, A. Andreev, and A. Pirogov, J. Alloys Compd. **581**, 423 (2013).